energies

MDPI

Article

Tip-Bed Velocity and Scour Depth of Horizontal-Axis Tidal Turbine with Consideration of Tip Clearance

Tianming Zhang [1,2], Wei Haur Lam [1,2,*], Yonggang Cui [1,2], Jinxin Jiang [1,2], Chong Sun [1,2], Jianhua Guo [1,2], Yanbo Ma [1,2], Shuguang Wang [1,2], Su Shiung Lam [3] and Gerard Hamill [4]

1 State Key Laboratory of Hydraulic Engineering Simulation and Safety, Tianjin University, Tianjin 300350, China; zhangtianming@tju.edu.cn (T.Z.); cui_yonggang@tju.edu.cn (Y.C.); jiangjinxin@tju.edu.cn (J.J.); chong@tju.edu.cn (C.S.); guojh@tju.edu.cn (J.G.); mayanbo@tju.edu.cn (Y.M.); wangsg@tju.edu.cn (S.W.)
2 First R&D Services, A-08-16 M Suites, 283 Jalan Ampang, 50450 Kuala Lumpur, Malaysia
3 Pyrolysis Technology Research Group, School of Ocean Engineering, Universiti Malaysia Terengganu, 21030 Kuala Nerus, Terengganu, Malaysia; lam@umt.edu.my
4 School of Natural and Built Environment, Architecture, Civil & Structural Engineering and Planning, Queen's University Belfast, David Keir Building, Stranmillis Road, Belfast BT9 5AG, UK; g.a.hamill@qub.ac.uk
* Correspondence: wlam@tju.edu.cn

Received: 12 April 2019; Accepted: 23 June 2019; Published: 25 June 2019

Abstract: The scouring by a tidal turbine is investigated by using a joint theoretical and experimental approach in this work. The existence of a turbine obstructs a tidal flow to divert the flow passing through the narrow channel in between the blades and seabed. Flow suppression is the main cause behind inducing tidal turbine scouring, and its accelerated velocity is being termed as tip-bed velocity (V_{tb}). A theoretical equation is currently proposed to predict the tip-bed velocity based on the axial momentum theory and the conservation of mass. The proposed tip-bed velocity equation is a function of four variables of rotor radius (r), tip-bed clearance (C), efflux velocity (V_0) and free flow velocity (V_∞), and a constant of mass flow coefficient (C_m) of 0.25. An experimental apparatus was built to conduct the scour experiments. The results provide a better understanding of the scour mechanism of the horizontal axis tidal turbine-induced scour. The experimental results show that the scour depth is inversely proportional to tip-bed clearance. Turbine coefficient (K_t) is proposed based on the relationship between the tip-bed velocity and the experimental tidal turbine scour depth. Inclusion of turbine coefficient (K_t) into the existing pier scour equations can predict the maximum scour depth of a tidal turbine with an error range of 5–24%.

Keywords: marine renewable energy; tidal power; tidal turbine-induced scour; turbine wake

1. Introduction

Tidal current energy is predictable compared to other renewable resources, which makes it a reliable source of such energy [1]. Tidal turbines are the main energy generating devices used to harness tidal power in various countries [2]. Scientists and engineers have conducted various investigations to push for tidal power to be available for mass utilization with cheaper electricity prices [3]. The seabed scouring of turbines is an important consideration for their design and application. The maximum scour depth is one of the main interests of engineers, and scour depth can be related to water depth, turbine blade numbers, and blade area ratios [4]. The existence of a turbine obstructs flow with its blockage effects, and turbine scouring is influenced by the tip clearance between blades and the seabed [5].

The understanding of tidal turbine scouring is limited for scientists and engineers. SeaGen in Strangford Loch, Belfast, is an important case of using a quad pile structure fixed on the seabed to support a tidal power system. Early researchers presumed that tidal turbine-induced scouring is analogous to bridge pier-induced scouring when a monopile support is used [4]. A tidal turbine scour is dominated by its monopile support interacting with the seabed. This scouring is caused by a horseshoe vortex at the upstream pile as well as the vortex shedding within the downstream wake [6]. Neill [7] proposed that the ratio of scour depth to the diameter of a pile is a constant value, and maximum scour depth is proportional to the pile diameter. Breusers et al. [8], Sumer et al. [9], and Richardson et al. [10] suggested that more parameters should be considered, including free flow velocity, water depth, bed condition, and the size of sediment, for the proposal of their enhanced equations based on Neill's proposal.

Propeller scouring is different than the scouring caused by a single cylinder. The rotating propeller produces a high velocity jet, and this jet is the main factor of active seabed scouring. Albertson et al. [11], Hamill [12], and Lam et al. [13] investigated velocity distribution within propeller wake and proposed wake distribution equations. Jiang et al. [14] proposed a theoretical model for a ship twin-propeller jet. The scour pattern induced by a propeller was attributed mainly due to the expansion of a propeller wake. Hamill et al. [15,16] studied propeller seabed scouring under various seabed conditions, as well as a scouring pattern with the existence of a quay wall to propose equations for estimating the maximum depth of a scouring with a quay wall. Cui et al. [17] proposed an empirical 2D scour model to predict the scour profile of a propeller.

A tidal turbine and propeller are both the rotating devices submerged underwater. The rotating propeller releases energy into the water through the production of forward thrust, and a turbine extracts energy from the water through rotations. Lam et al. and Ma et al [18,19] found that strong shadowing effects appeared on the turbine through the analysis of experimental and numerical results. Chen and Lam [5] studied the shadowing effect of a turbine rotor and showed that the velocity of a slipstream is accelerated by about 105%. Previous studies have suggested the presence of tidal turbine effects on seabed scouring [20–23]. Giles et al. [24] showed that flow is suppressed due to blockage and accelerates to balance mass flow and velocity. Wang et al. [25] proposed efflux velocity equations by fitting an energy coefficient equation with a tip speed ratio.

This study was aimed to determine the effects of a rotating turbine on seabed scouring. A tip-bed velocity equation is proposed to predict the accelerated velocity in between the blades and seabed, with a consideration of the mass flow coefficient (C_m) based on the axial momentum theory and the conservation of mass. Experiments were conducted to investigate tidal turbine scouring with a consideration of tip clearances. An empirical equation is proposed to estimate the maximum scour depth.

2. Tip-Bed Velocity Used for Seabed Scouring

The tip-bed velocity between a tidal turbine and the seabed is the main factor in seabed scouring around tidal turbine structures. Tip-bed flow is squeezed and accelerated due to the existence and blockage of a rotating turbine. Flow suppression increases the velocity within the channel and in between the blades and seabed. This accelerated velocity in the region between the blades and turbine is termed the tip-bed velocity, a concept which can lead to a more severe scour. We propose a tip-bed velocity equation to predict the velocity between the tidal turbine and seabed based on the axial momentum theory and conservation of mass.

2.1. Tip-Bed Velocity Equation

A minimum efflux velocity appears at the outflow plane of a tidal turbine due to the extraction of energy. Equations to predict efflux velocity were proposed by Albertson et al. [11], Hamill et al. [26], and Lam and Chen [27] based on the axial momentum theory. The turbine is considered an actuator

disc under assumptions in axial momentum theory. Figure 1 shows the effect of an actuator disc model on the flow pattern in one direction.

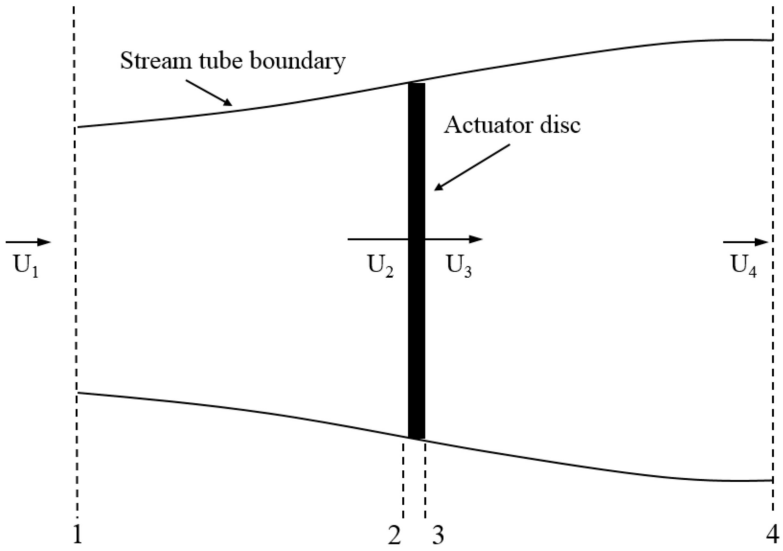

Figure 1. An actuator disc model applied on a tidal current turbine.

The axial momentum theory assumes no energy losses in fluid motion, and the Bernoulli equation can be applied to balance energy in the upstream regions (far upstream (location 1) and immediately upstream (location 2)) and downstream regions (immediately downstream (location 3) and far downstream (location 4)), as shown in Figure 1. Equation (1) shows the relationship between the pressure potential energy and kinetic energy upstream of the actual disc (locations 1 and 2).

$$P_1 + \frac{1}{2}\rho {U_1}^2 = P_2 + \frac{1}{2}\rho {U_2}^2 \quad (1)$$

Equation (2) shows the relationship between the pressure potential energy and kinetic energy downstream of the actuator disc (locations 3 and 4).

$$P_3 + \frac{1}{2}\rho {U_3}^2 = P_4 + \frac{1}{2}\rho {U_4}^2 \quad (2)$$

where ρ is the density of fluid (kg/m^3); P_1, P_2, P_3, and P_4 are the pressure (Pa); and U_1, U_2, U_3, and U_4 are the axial velocity (m/s). The thrust acted at the actuator disc is produced due to the pressure difference (P_2, P_3) between front and back surfaces in Equation (3). The free flow has energy losses when passing through the actuator disc.

$$T = A(P_2 - P_3) \quad (3)$$

where T is the thrust force (N), A is the area of the actuator disc (m^2), and P_2 and P_3 are the pressures located at the immediate upstream and immediate downstream (Pa).

Pressure is assumed to be equal ($P_1 = P_4$) far upstream and far downstream, and fluid velocity is equal ($U_2 = U_3$) when immediately passing through the actuator disc due to continuity. Equation (4) can be obtained by solving (P_2–P_3) using Equations (1)–(3).

$$T = \frac{1}{2}\rho A({U_1}^2 - {U_4}^2) \quad (4)$$

The thrust function (T) with thrust coefficient (C_T) of tidal turbine in Lam et al. [18] is presented in Equation (5) as an alternative to balance Equation (6).

$$T = C_T \rho A {U_1}^2 \tag{5}$$

$$C_T \rho A {U_1}^2 = \frac{1}{2} \rho A ({U_1}^2 - {U_4}^2) \tag{6}$$

The efflux velocity equation in Lam et al. [18] is obtained through the rearrangement of Equation (6) to predict the efflux velocity (V_0), as shown in Equation (7).

$$V_0 = V_\infty \sqrt{1 - C_T} \tag{7}$$

where V_0 is efflux velocity (m/s), which is equal to U_4 in the Equation (6). V_∞ is the free flow velocity (m/s) which is equal to U_1 in Equation (6)

A narrow region is formed between the turbine and seabed when the turbine is close to the seabed. The existence of rotating turbine disturbs the natural water flow by blocking partial water and extracting energy with velocity reduction with a complicated wake downstream and accelerated tip-bed velocity, which is generally called as shadowing effect. The shadowing effect of a tidal turbine is the main influencing factor on tidal turbine scouring. The squeezing process of tip-bed velocity is shown in Figure 2. The tip-bed velocity of this squeezed flow is accelerated by the shadowing effect of tidal turbines [5]. The aforementioned axial momentum theory is combined with the conservation of mass to estimate the tip-bed velocity.

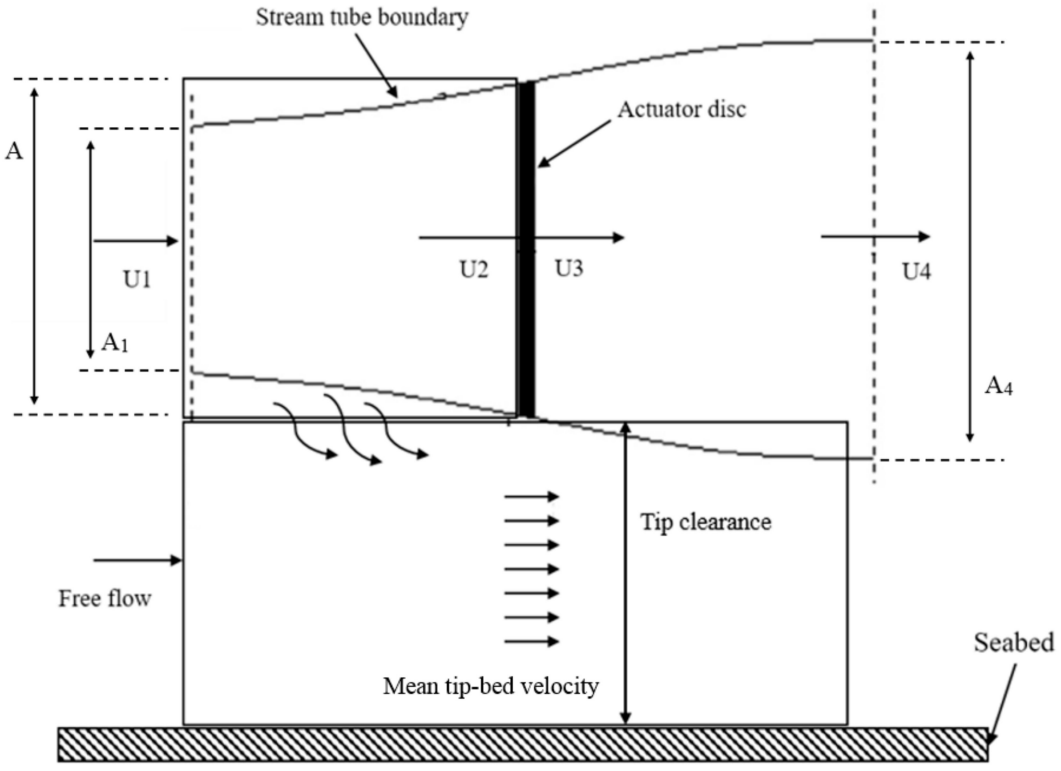

Figure 2. Squeezing process of the tip-bed velocity in scouring.

Partial free flow passes through the actuator disc, and the other flow spreads around due to the shadowing effect of rotating turbines. Equation (8) shows the mass flow pass through a turbine in a unit time.

$$m = \rho U_{2/3} A = \rho U_1 A_1 \tag{8}$$

where m is the mass flow rate (kg/s), ρ is the density of fluid (kg/m^3), $U_{2/3}$ is the axial velocity immediate upstream or immediate downstream (m/s), A is the area of the actuator disc (m^2), U_1 is the axial velocities far upstream (m/s), and A_1 is the area of water flowing through the actuator disc at location 1 (m^2). Equation (9) shows the total mass flow rate far upstream in area A, which is same as the area of the actuator disc, as shown in Figure 2

$$m_1 = \rho U_1 A \tag{9}$$

where m_1 is the total mass flow rate in area A at location 1 (kg/s). Free flow diffusion occurs due to the shadowing effect of the actuator disc within area A, as shown in Figure 3, which leads to the acceleration of the surrounding flow. Equation (10) shows the mass flow that does not pass through the actuator disc.

$$\Delta m = \rho U_1 A - \rho U_1 A_1 = \rho U_1 A - \rho U_{2/3} A \tag{10}$$

where Δm is the mass flow rate that does not pass through the actuator disc (kg/s).

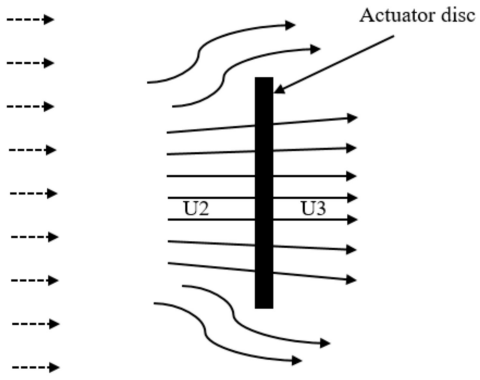

Figure 3. Flow diffusion due to the shadowing effect of the actuated disc.

The fluid that does not pass through the actuator disc can be represented by U_1 and U_4 through energy analysis in order to rearrange and simplify Equation (10). Equation (11) shows the extracted energy by a tidal turbine.

$$\Delta P = \mathrm{TU} = m(U_1 - U_4)U_{2/3} \tag{11}$$

where ΔP is the extracted energy of tidal turbine and m is the mass flow rate through a turbine (kg/s). Energy changes after the flow passes through a turbine. The change of energy can be regarded as the energy extracted by the turbine, as shown in Equation (12).

$$\Delta P = \frac{1}{2} m({U_1}^2 - {U_4}^2) \tag{12}$$

Equation (13) is obtained by balancing the energy in Equations (11) and (12).

$$U_{2/3} = \frac{1}{2}(U_1 + U_4) \tag{13}$$

The mass flow rate that does not pass through the tidal current turbine (Equation (10)) can be represented by inserting $U_{2/3}$ of Equation (13), as shown in Equation (14).

$$\Delta m = \rho\left(\frac{(U_1 - U_4)}{2}\right)A \tag{14}$$

The flow that does not pass through the tidal turbine is spread around due to the shadowing effect of tidal current turbines, as shown in Figure 3. Downward flow is mixed with free flow in the tip-bed region, which leads to an increase in tip-bed velocity compared to the undisturbed free flow. The mass flow coefficient C_m is proposed to present the ratio of Δm_1 (flow mass passing through the mixing area)

to Δm (the total mass that does not pass through the tidal turbine), as shown in Equation (15). The mixing area is shown in Figure 4. The mass flow coefficient C_m is related to turbine parameters, tip clearance, water depth, turbulence intensity, and seabed conditions. This assumes that the water can flow downward, upward, leftward, and rightward, and 25% of the water is flowing downward into the mixing area. A mass flow coefficient C_m of 0.25 is taken to represent the downward water.

$$C_m = \frac{\Delta m_1}{\Delta m} \tag{15}$$

where C_m is the mass flow coefficient and Δm_1 is the downward mass flow (kg/s).

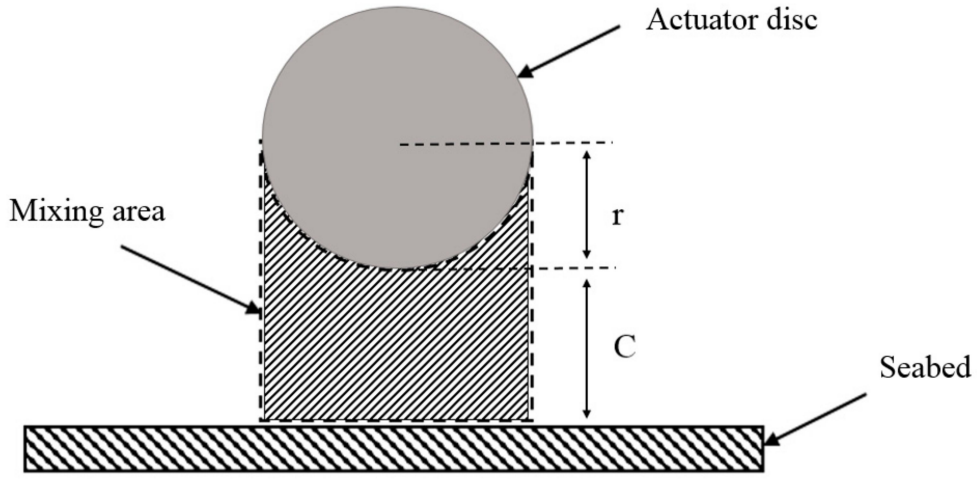

Figure 4. Mixing area calculated in the predicted equation.

Equation (16) shows the mass flow passing through the mixing area. The left hand side is the mass flow passing through the mixing area upstream. The right hand side is the mass flow which represents the tip-bed velocity. A tip-bed velocity equation is proposed by rearranging Equation (16), as shown in Equation (17).

$$V_\infty \rho\left((C+r)2r - \frac{\pi r^2}{2}\right) + C_m\left(\frac{V_\infty - V_0}{2}\right)\rho\pi r^2 = V_{tb}\rho\left((C+r)2r - \frac{\pi r^2}{2}\right) \tag{16}$$

$$V_{\mathrm{tb}} = V_\infty + \pi C_m r\left(\frac{V_\infty - V_0}{4C + (4-\pi)r}\right) \tag{17}$$

where r is the radius of the actuator disc (m), C_m is mass flow coefficient, C is the tip clearance between the turbine and seabed (m), V_{tb} is the tip-bed velocity (m/s), V_0 is the efflux velocity (m/s), and V_∞ is the free flow velocity (m/s).

2.2. Comparison

Chen and Lam [5] investigated the slipstream between the seabed and the marine current turbine via OpenFOAM. Figure 5 shows the comparison between the proposed tip-bed velocity equation and the previous works. The mass flow coefficient C_m is theoretically taken as 0.25. The tip-bed velocity is 1.46 V_∞ in theory when the tip clearance is zero. Theoretical work shows the maximum increment of the tip-bed velocity is 46% of the free flow velocity due to blockage effects. The application range of the tip-bed velocity equation is for a tip clearance of more than 0.4 D_t. The maximum variation of 3.06% occurred at 0.4 D_t for the tip clearance in the range 0.4–1.0 D_t, as shown in Table 1.

The proposed equation fits better in bigger tip-bed clearance areas compared to previous works. The variation increases in smaller tip-bed clearance. The discrepancy may be due to the influence of mass flow coefficient C_m in the calculation of tip-bed velocity. It is assumed that 25% of water flows

downward into the mixing area. Actually, C_m depends on many turbine parameters, and various values of C_m at different tip-bed clearances should be proposed in future.

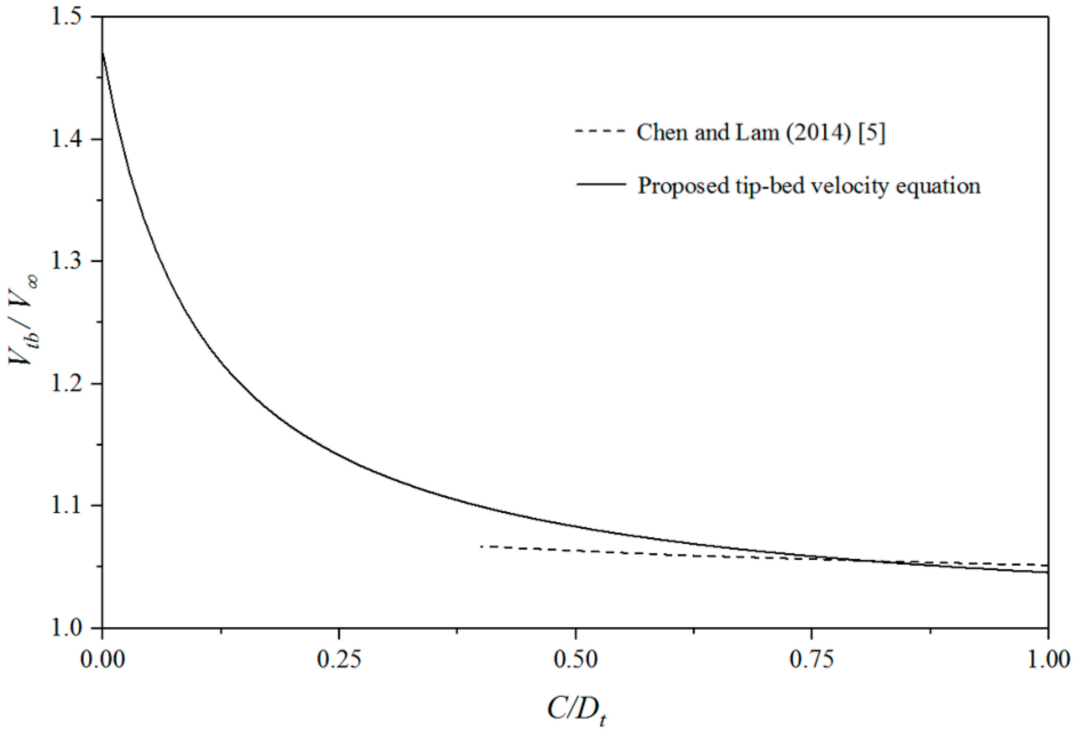

Figure 5. Comparison of predicted tip-bed velocity with previous research.

Table 1. The tip-bed velocity of our proposed equation and previous works.

Tip Clearance (C/D_t)	Proposed Equation (V_{tb}/V_∞)	Previous Works (V_{max}/V_∞)	Variation (%)
1.0 D_t	104.56	105.25	−0.50
0.8 D_t	105.57	105.53	0.03
0.6 D_t	107.14	106.00	1.07
0.4 D_t	109.96	106.69	3.06

3. Scour Experiment

3.1. Purposed-Built Apparatus

A series of scour experiments were carried out in the Marine Renewable Energy Laboratory at Tianjin University, P.R. China. The experimental flume was a purpose-built horizontal recirculating flume used to model the tidal flow in the actual conditions. This flume was 1.8 m in length, 0.8 m in width, and 0.6 m in height, as shown in Figure 6. An inner separator was used to produce a recirculating channel with a 0.25 m width. The flume was a patented invention of a horizontal recirculating flume for a tidal-current-turbine by Lam et al. [28], with an application number of 2016107047703CN. Perspex panels were used for both sides of the recirculating flume to allow for transparent observations from the side view during experiments. The flow recirculation was driven by a propeller submerged into the water channel (as shown in label 2 in Figure 6). The turbine model was positioned at opposite sides of the flume to investigate its induced scouring. A pitot tube was used to measure the mean velocity to determine the incoming flow speed in the recirculating flow. The free flow velocity in the water channel could be adjusted by controlling the rotational speed of a propeller. The turbine was made via 3D-printing, using a polylactic acid (PLA) material with an accurate curvature blade, as shown in

Figure 7. The rotation of the turbine model was driven by a direct current (DC) motor connected to a universal joint to allow for 90° of torque transmission.

Figure 6. Recirculating flume in Marine Renewable Energy Laboratory, Tianjin University. (1: Plexiglass; 2: Propeller; 3: Laser range finder; 4: Guide bend; 5: Frame structure; 6: Separator; 7: Flume; 8: Perforated distribution plate; 9: Sand box).

Figure 7. 3D printed turbine model and monopile structure for the scouring experiment.

Sediment was filled into a sand box, which was 0.25 m in width, 1 m in length, and 0.1 m in depth, to model the seabed (located at label 9 in Figure 6). The sand box was used to locate the sand at the designated location in the flume bed and was easy to remove after experiments. The upstream and downstream areas of the sandbox had slopes to ensure that the flow passed through the measurement area smoothly. A flat plate was fixed on the head of the sand box. The combination of a slope plate and a flat plate made the flow pass through the test section smoothly in the scouring process. The sand was filled in the box and was levelled by using a sand leveller before the scour experiments. A monopile support structure was embedded into the middle of the sandbed during the tests. Sands with a median particle size of d_{50} = 1 mm were used in the experiments to keep the scouring condition of clear water, as shown in Figure 8, which ensured that the incoming flow velocity near the seabed ($u^* \approx 0.013$ m/s) was below the incipient velocity of sediment ($u_c^* \approx 0.023$ m/s for the sediment with a diameter d_{50} = 1.0 mm. The critical Shields parameter was 0.034).

The turbine used in the experiment was a three-bladed horizontal-axis turbine. The rotor diameter was 0.08 m, and the pitch angle was 15°. These parameters of the blades were obtained from the performance test of a tidal turbine based on Bahaj et al. [29], which was a 1:10th geometric scaling model. In this paper, the free flow velocity applying Froude similitude was 0.22 m/s. Four types of Reynolds number were provided on the basis of facility, the tidal turbine, and the cylinder structure [30–32]. Detailed flow parameters of the flume and tidal turbine are shown in Table 2.

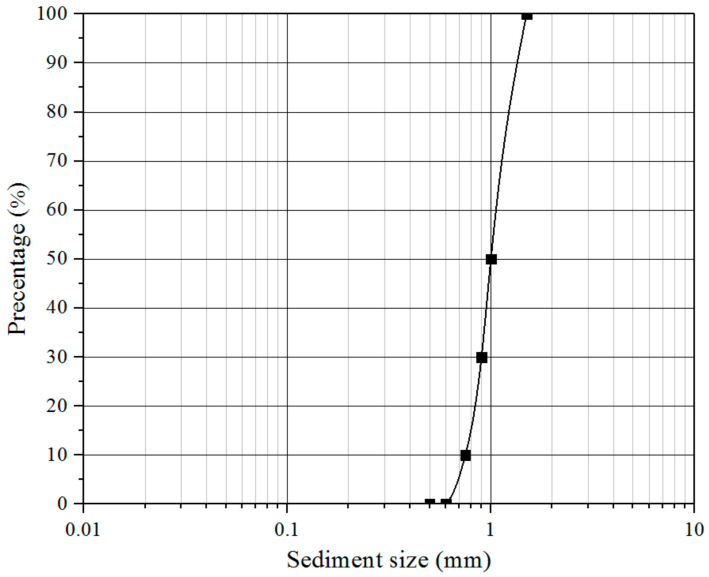

Figure 8. Particle size distribution of seabed scour sand.

Table 2. Flow parameters of the flume and tidal turbine.

Flow Parameters	Bahaj et al. [29]	1:10th Scaled Model
Rotor diameter (D_t)	0.8 m	0.08 m
Flow depth (h_f)	1.2 m	0.25 m
Free flow velocity (V_∞)	0.7 m/s	0.22 m/s
Depth-based Reynolds number (Re_{hf})	8.4×10^5	0.55×10^5
Chord-based Reynolds number ($Re_{0.7}$)	7.9×10^4	0.25×10^4
Radius-based Reynolds number (Re_∞)	5.6×10^5	0.18×10^5
Cylinder-based Reynolds number (Re_{Ds})	—	2200
Froude number (Fr)	0.25	0.25
Tip Speed Ratio (TSR)	5	5
Rotational speed (RPM)	84 rpm	263 rpm

Four groups of experiments were conducted at various tip clearances to investigate the seabed scouring of a tidal turbine, as listed in Table 3. The seabed scour depth was measured at time = 2 min, 15 min, 30 min, 60 min, and 120 min. Water recirculation in the flume was stopped during the scour depth measurement. The seabed scour depth was measured by using a laser range finder. The propeller continued to drive the water circulation after the completion of each measurement. According to the work of Whelan et al, the blockage ratio ($B = A/bh$) was 0.04 in the recirculating flume, which was effectively unblocked [33]. The diameter of the turbine was much smaller than the width of the water channel with 1 D_t space to the edges of flume. The tidal turbine was submerged at 2 D_t underwater. Thus, the impacts of boundary effects and water free surface were assumed insignificant during seabed scour experiments.

Table 3. Experimental parameters used in turbine scouring.

Experimental Parameters	Details
Rotor diameter (D_t)	0.08 m
Hydrofoil	NACA 63-8XX
Number of blades (N)	3
Tip clearance (C)	0.25 D_t, 0.50 D_t, 0.75 D_t, 1 D_t
Tip speed ratio (TSR)	5
Rotational speed (RPM)	263 rpm
Coefficient of thrust (C_t)	0.825
Direction of rotation	Anti-clockwise
Support structure diameter (D_s)	0.01 m
Free flow velocity (V_∞)	0.22 m/s
Water depth (h_f)	0.25 m
Water channel width (L_w)	0.25 m
Mean sediment grain diameter (d_{50})	1.0 mm

3.2. Flow Disturbance and Perturbation

Flow disturbance and perturbation were mainly caused by the water circulation in the channel. The bend of the water channel caused the outer flow (flow close to the outer section) to move faster than the inner flow (flow close to the inner section) due to centrifugal forces. Before the seabed scouring experiment, velocity measurements were carried out at four transverse sections upstream of the turbine (Figure 9), and these were used to investigate the incoming flow structure and its turbulent level.

The distribution of axial velocity was complicated at Section 1 of Figure 9a due to the combined effects of water motion in the bending region and the propeller wake as shown in Figure 10a. A perforated distribution plate (Figure 6, label 8) with square grids was fitted to break the turbulence structures and to remove the large scale eddies caused by the flow direction change in the bending region. This produced a continuous flow with uniform velocity distribution at the inlet of the test section. The size of the square grids is generally calculated using the empirical Equation (18) [34].

$$\frac{M}{d} = 5\text{–}10 \tag{18}$$

where M is the width of the water channel (m) and d is the width of the square grids on the perforated distribution plate (m). The velocity distributions at the horizontal and vertical sections in the water channel are presented in Figure 10a,b. The velocities in the x-axis are non-dimensionalised by the free flow velocity (V_∞). The y-axis in Figure 10a,b represent the distances along the horizontal and vertical sections, respectively, and are non-dimensionalised by the channel depth (L_d) and the channel width (L_w).

The axial velocity profile at Section 1 shows that the turbulent level was significant in the turning point, and the velocity distribution was non-uniform compared to the following downstream Sections 2–4, as shown in Figure 10a. The flow was smoothened to be more uniform after passing through the perforated distribution plate at Section 2. The mean velocity was slightly increased at Section 3 compared to Section 2 due to the existence of the sand box. The sand box reduced the water height to accelerate the flow in the channel due to continuity effects. The velocity difference between the outer flow and inter flow at Sections 2 and 3 was much greater than Section 4. It can be seen that the velocity difference between the inner and outer flows decreased downstream and reached a close to uniform flow at 1 D_t upstream. The maximum difference of velocity was insignificant, with only 0.01 m/s for the inner and outer flows at Section 4. A vertical velocity distribution in the z direction was located at Section 4, as shown in Figure 10b. Vertical lines 1 and 3 were located at the left/outer side and right/inner side of the cross section respectively and the vertical line 2 was located at the middle, as shown in Figure 9b. It should be noted that the zero point in z direction was located at seabed.

The influence of water depth was insignificant, with a maximum velocity difference of only 0.02 m/s due to seabed effects. The flume was presumed to provide uniform flow for the experimental investigation.

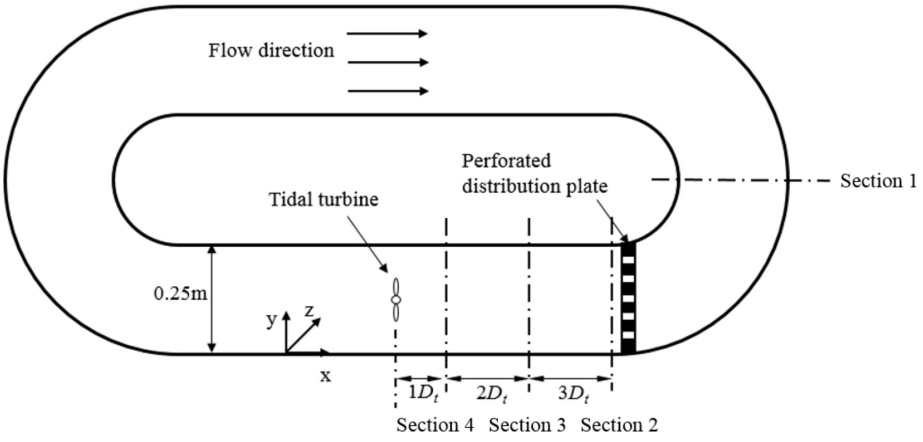

(**a**)

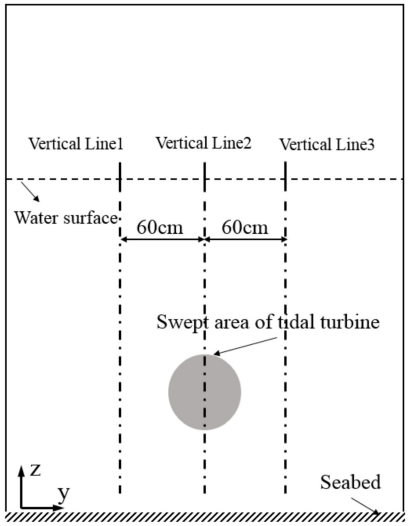

(**b**)

Figure 9. Position of velocity measurements: (**a**) Transverse sections. (**b**) Vertical Lines at Section 4.

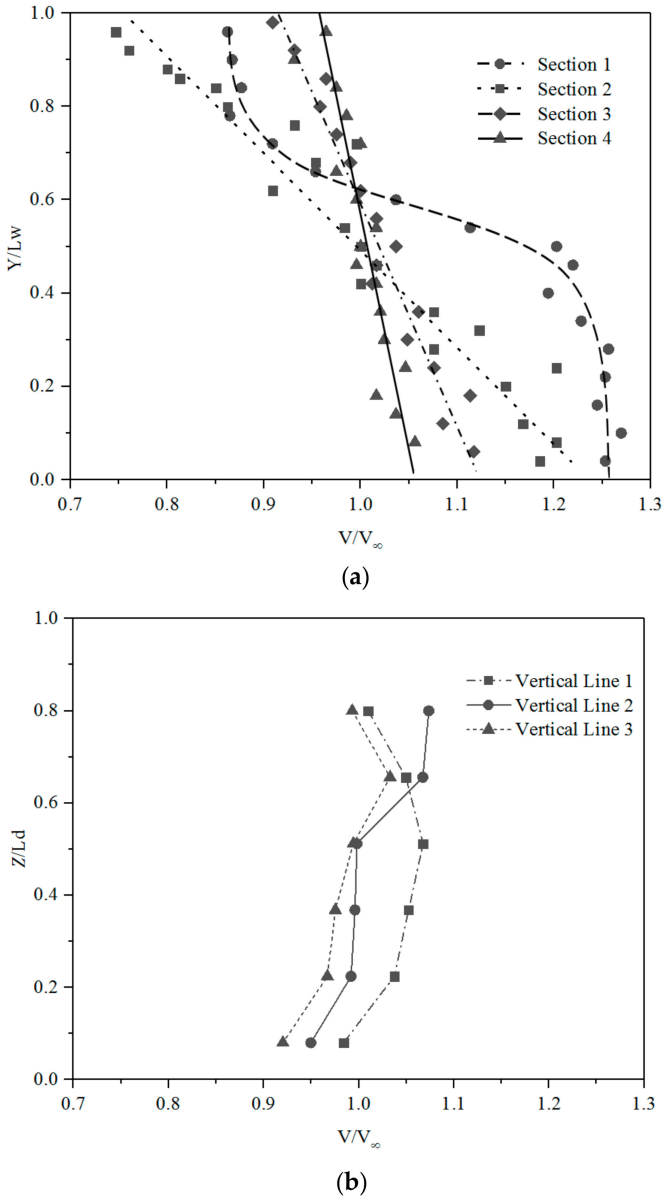

Figure 10. Velocity distributions at different locations: (**a**) Horizontal section along the channel width. (**b**) Vertical section along the channel depth.

4. Results and Discussion

Seabed scouring experiments for turbines were conducted to better understand the influences of the shadowing effect on seabed scouring at different tip clearances. The experiment results were recorded at the times of 2 min, 15 min, 30 min, 60 min, and 120 min. The heights of the turbine position were set at the tip clearances of 0.25 D_t, 0.50 D_t, 0.75 D_t, and 1.00 D_t.

4.1. Seabed Scour Profile

Tidal turbine scouring has an analogous profile and moving trend compared to cylinder scouring, as shown in Figure 11. The maximum scour depth for a tidal turbine with clearances C/D_t = 0.5 and 1.0 was compared to the cylinder scouring experiments by Zhao et al. [35], Kitsikoudis et al. [36], and Yao et al. [37], as listed in Table 4. The monopile-supported tidal turbine scouring was analogous to the single monopile when its turbine was placed at a position with sufficient height. The influence of the rotating turbine was significant to the seabed at a low clearance condition, but it was insignificant

for a high clearance. The maximum scour depth for a tidal turbine with a tip clearance of 1.0 D_t was 0.9 D_s, which is close to the cylinder scour depth of 1.11 D_s, 1.0 D_s, and 1.0 D_s found by Zhao et al. [35], Kitsikoudis et al. [36], and Yao et al. [37], respectively. The tidal turbine had a deeper scour pit compared to the cylinder monopile when the tip clearance of the tidal turbine was small, which was 0.5 D_t in the current work. The scouring range of the sand pit caused by the tidal turbine with a tip clearance of 1.0 D_t was almost the same as the cylinder scour. However, the sand dune profile was different for various cases. The tidal turbine-induced sand dune was higher compared to the cylinder due to the participation of turbine wake. The free flow velocity and scouring time also had significant impacts on the height of the sand dunes.

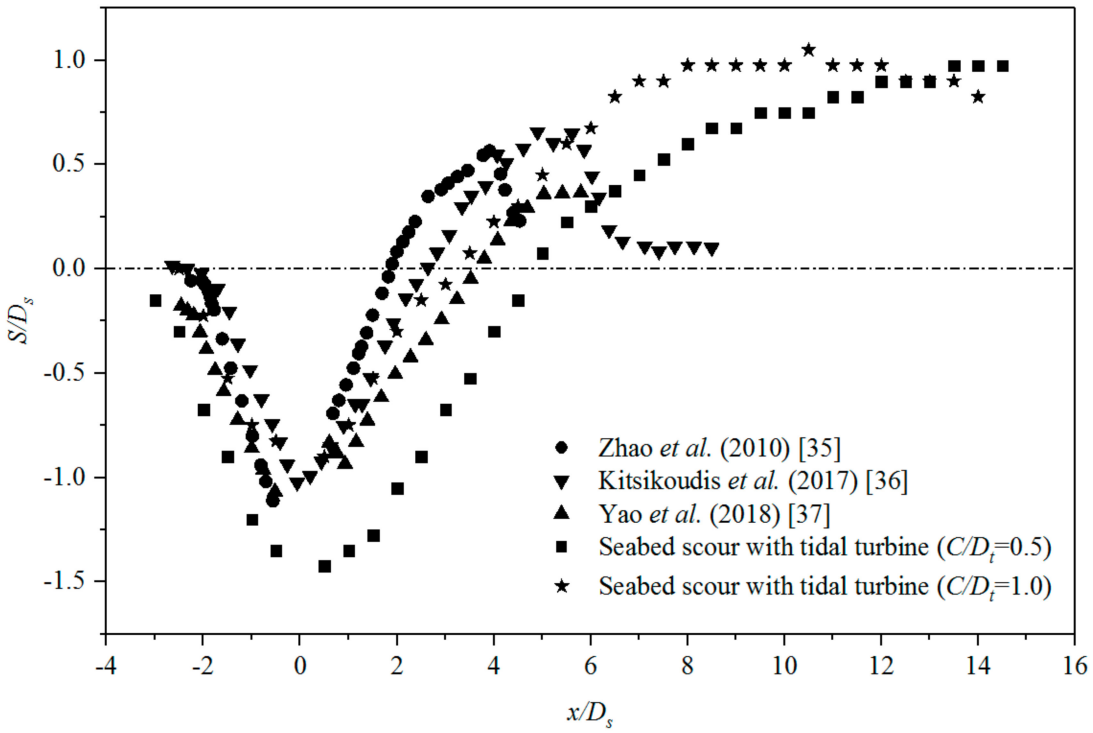

Figure 11. Tidal turbine scouring and cylinder scouring.

Table 4. Comparison of tidal turbine scouring and cylinder scouring.

Scour Parameters	Tidal Turbine Scour		Cylinder Scour		
	C/D_t = 0.5	C/D_t = 1.0	Zhao et al. (2010) [35]	Kitsikoudis et al. (2017) [36]	Yao et al. (2018) [37]
Scour depth	1.42 D_s	0.9 D_s	1.11 D_s	1.0 D_s	1.0 D_s
Length of sand pit	7.5 D_s	5.5 D_s	4.06 D_s	4.72 D_s	5.97 D_s
Height of sand dunes	0.976 D_s	1.05 D_s	0.56 D_s	0.65 D_s	0.36 D_s

Lam et al. [18], Chen [38], and Hill et al. [22] analysed the shadowing effect of tidal turbines on seabed scouring. Figure 12 shows a comparison between the current experimental results and those of Chen [38], Hill et al. (live bed and clear water scour) [22], and Zhao et al. (cylinder scour) [35].

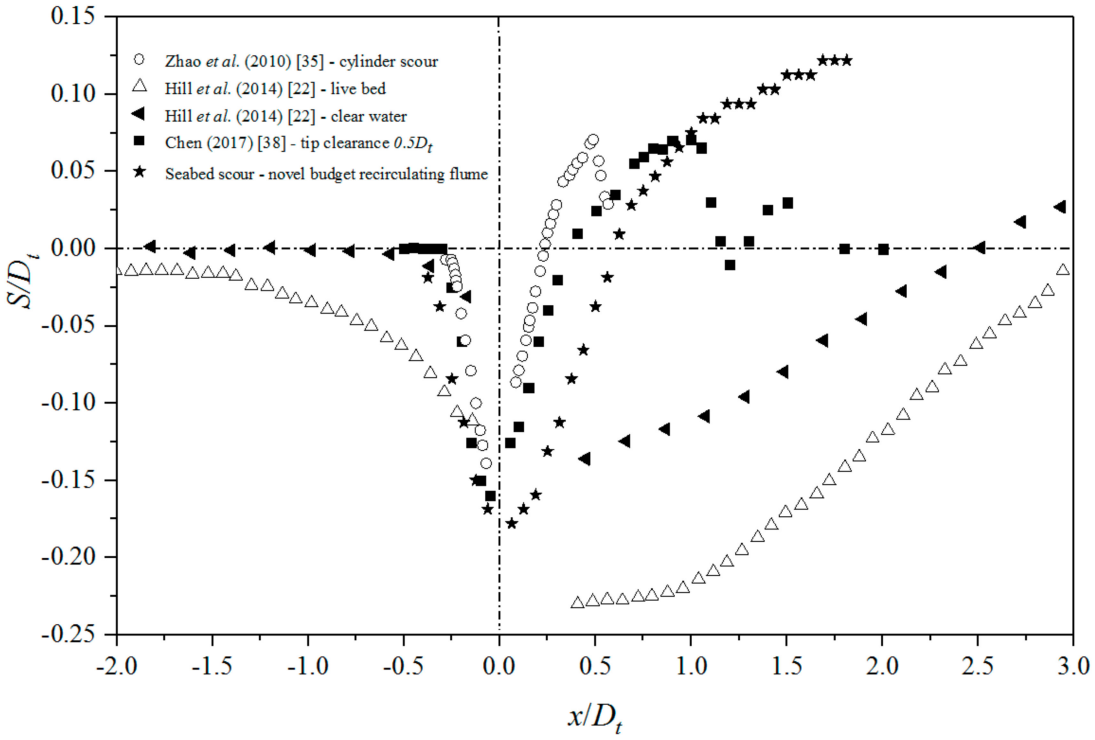

Figure 12. Comparison of scouring profiles.

The maximum scour depth in the recirculating flume (S = 0.177 D_t) was only 8% deeper than the seabed scour depth found by Chen (S = 0.165 D_t) [38]. The rear boundary of the scour pit was moved backward compared that found by Chen [38], which may be due to the effects of a higher turbulence intensity at the rear of the tidal turbine. Chen [38] used a tip speed ratio (TSR) = 3.67 for all cases, and the current works used TSR = 5. Turbulence intensity may cause excessive vortex shedding at the rear of a tidal turbine with the higher TSR, leading to seabed scour pit was more expansive than Chen [38]

Our tidal turbine-induced scour profile is slightly different than that of Hill et al. [22] in both clear water and live bed sediment transport experiments. It should be noted that the turbine was only submerged at 0.5 D_t in the Hill et al. [22], and the tidal turbine was submerged at 2 D_t in this work. The difference in position of the submerged turbine caused the different scour depths due to the influence of the free water surface. Hill et al. [22] indicated that their mean water surface elevations indicated a maximum peak-to-trough oscillation at the rotor location of approximately 2–3% of the flow depth with the turbine effect on the free surface. The oscillation of the free surface led to the length extension of the seabed scour pit. The maximum seabed scour depth in live-bed conditions (Hill et al. [22] had a scour depth of S = 0.24 D_t) is usually deeper than that of clear water scouring (novel recirculating flume scour depth, S = 0.177 D_t).

4.2. Scouring Process

Seabed scouring is mainly caused by the obstruction of a support structure and the shadowing effect of a rotating tidal turbine. Figure 13 shows the evolution of the scouring process of tidal turbines with support structures. The vortex scale is small in the initial stage, but its effect on local scouring is obvious. This indicates that the scouring process was strong at the initial stage, and a scour pit was quickly formed around the cylinder. The sand dune was deposited at the rear of the cylinder. The experiment showed that the depth of the scour reached about 60% of the stabilisation stage in the first 15 minutes. During the development stage, the depth of the seabed scour consistently increased with time, and the width of the pit was expanded. A sharp edge was formed at the tail of sand dunes, and the height of sand dunes kept increasing. During the stabilisation stage, the depth of the sand pit was no longer changed. The shear stresses and turbulence disturbance were no longer significant to

the motion of sediment particles in the scour pit. The scour depth tended to reach the limit. Though the scour pit was balanced, the sand dunes continued to move downstream. The sand dunes were continuously scoured and gradually approached the seabed as the scouring proceeded.

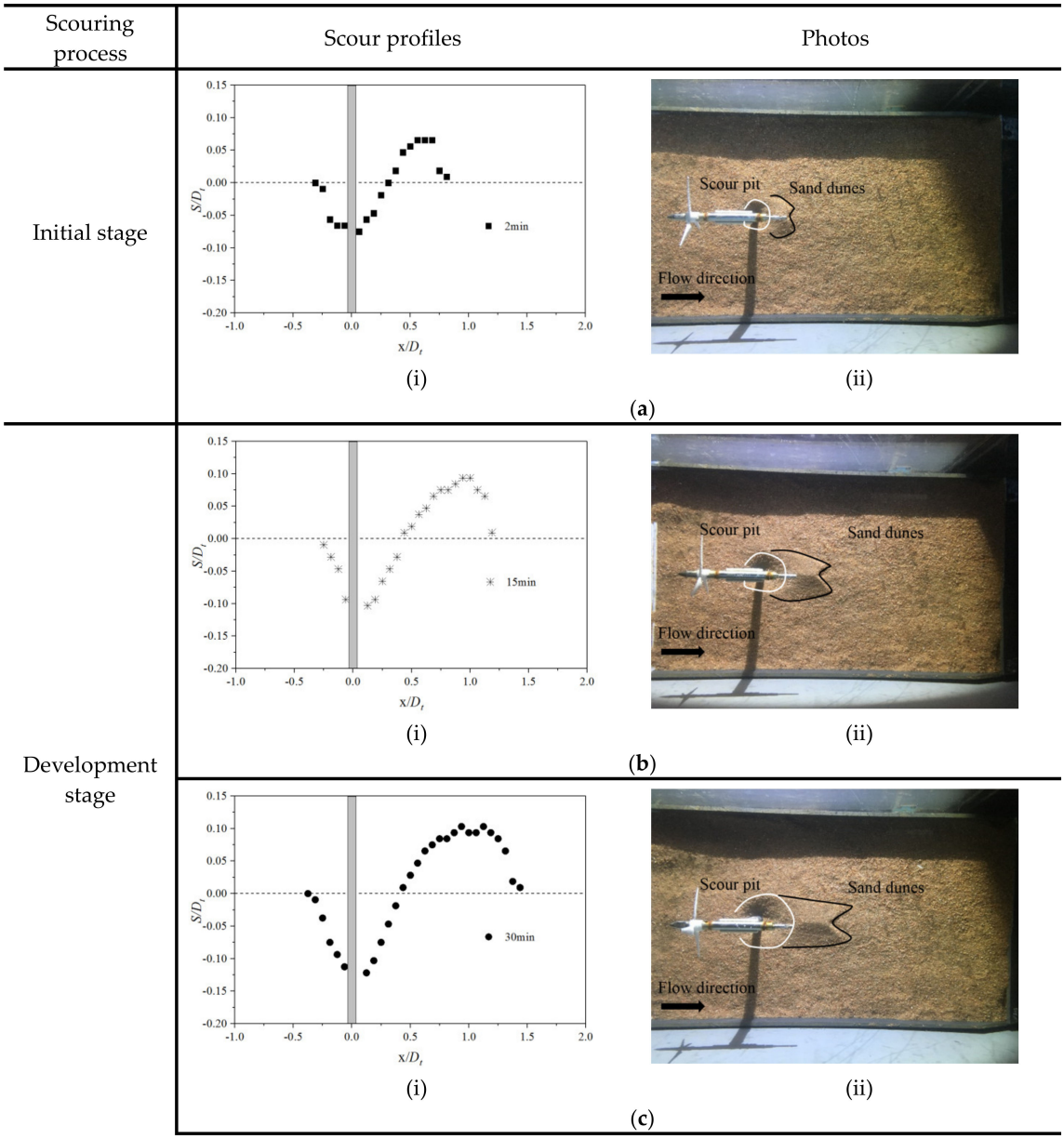

Figure 13. *Cont.*

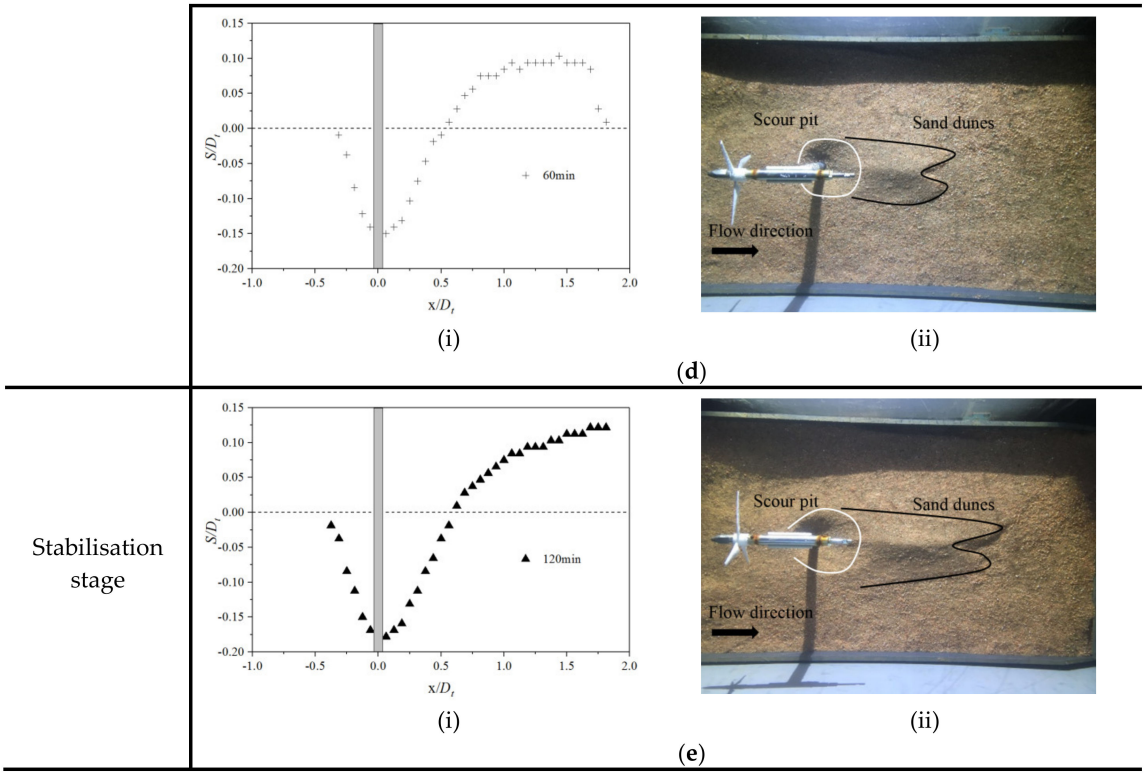

Figure 13. Scour patterns with the scouring process with times: (**a**) Time = 2 min. (**b**) Time = 15 min. (**c**) Time = 30 min. (**d**) Time = 60 min. (**e**) Time = 120 min.

Figure 14 shows the maximum scour depth of the tidal turbine under different tip clearances. Tidal turbine scour depth is inversely proportional to tip clearance. Larger scour depths occur with the smaller clearances. The increase of scour depth occurred obviously in between 0.50 D_t and 0.80 D_t with the decrease of tip clearance, while the scour depth maintained for the further reduction of clearance. When the tip clearance was shorter than 0.50 D_t, the flow in the gap between the turbine and seabed no longer need to be accelerated intensely. Less blocked water was diverted into the narrow region when tip clearance was shorter than 0.50 D_t. The same shadowing effect occurred when the clearance was smaller than 0.50 D_t. The scour depth kept constant at various lower tip clearances. Meanwhile, the shadowing effect had less influence on the tidal turbine scouring when the turbine position was sufficiently higher than 1.00 D_t.

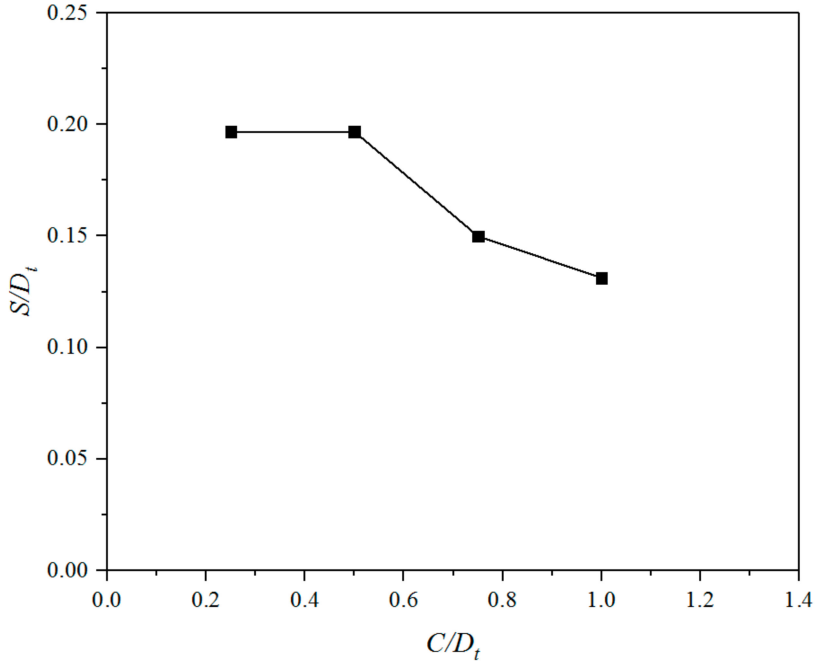

Figure 14. Seabed scour depth at different tip clearances.

The sand dune had a reverse trend compared to the sand pit, as shown in Figure 15. The sand pit depth increased with the decreasing of the tip clearance, but the sand dune height decreased with the decreasing of the tip clearance. The decrease of sand dune height was due to the vortex formed at a lower turbine position. For the lower turbine position, a large amount of sediment was scoured from the sand pit and deposited to form sand dunes. The sediment deposited at the sand dune was further scoured downstream due to the effect of the turbine position. The upstream edge of the scour pits occurred at $x/D_t = 0.35$. The position of upstream edge had an insignificant difference for various tip clearances. The downstream edge of the scour pits moved further downstream with smaller tip clearances.

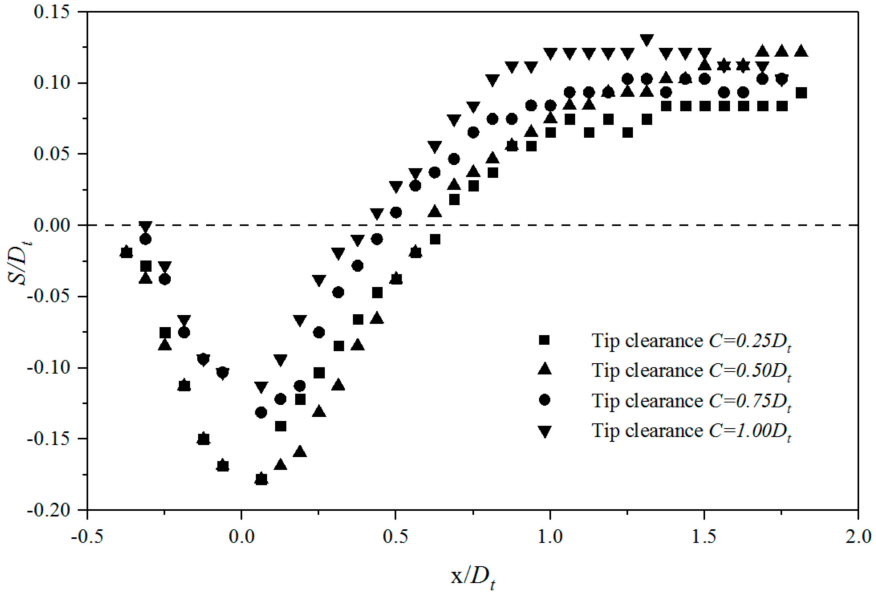

Figure 15. Scour profiles at different tip clearances.

5. Equation Used to Predict Maximum Scour Depth for Tidal Turbine

The seabed scour of the horizontal-axis tidal turbine was more severe than the cylinder scour mainly due to the shadowing effect of a rotating turbine. Neil [7], Breusers et al. [8], Richardson et al. [10], and Raaijmakers and Rudolph [39] proposed numerous equations to estimate the scour depth of a pier or pile, as shown in Table 5 and Appendix A. In this paper, the equations were based on the development of a pier or pile to predict the maximum scour depth for a tidal turbine.

Table 5. Equations used to predict the pile or pier scour.

Previous Works	Pile or Pier Scour Equation	Proposed Turbine Scour Equation
Neil (1973) [7]	$\frac{S}{D} = K_s$	$\frac{S}{D} = K_s K_t$
Breusers et al. (1977) [8]	$\frac{S}{D} = 1.55 K_s K_\theta K_b K_d tanh\left(\frac{h}{D}\right)$	$\frac{S}{D} = 1.5 K_s K_\theta K_b K_d tanh\left(\frac{h}{D}\right) K_t$
Richardson et al. (1993) [10]	$\frac{S}{D} = 2.0 K_s K_\theta K_b K_d K_w \left(\frac{h}{D}\right)^{0.35} {F_r}^{0.43}$	$\frac{S}{D} = 2.0 K_s K_\theta K_b K_d K_w \left(\frac{h}{D}\right)^{0.35} {F_r}^{0.43} K_t$
Raaijmakers and Rudolph (2008) [39]	$\frac{S}{D} = 1.5 K_v K_h tanh\left(\frac{h}{D}\right)$	$\frac{S}{D} = 1.5 K_v K_h tanh\left(\frac{h}{D}\right) K_t$

Neil [7] proposed a simple equation with the ratio of scour depth to the pile diameter as a constant K_s. K_s is correction factor for a pier nose shape. In this work, a turbine coefficient (K_t) in Equation (19) is proposed to predict the maximum tidal turbine scour depth. K_t is considered as the effect of a tidal turbine on scouring, which is related to the tip-bed velocity due to the existence of a rotating turbine.

$$\frac{S}{D} = K_s K_t \tag{19}$$

where S is the scour depth for turbine (m), D is the diameter of the support structure (m), K_s is the correction factor of the pier shape, and K_t is correction factor of turbine.

In this study, the seabed scouring of the tidal turbine was under the clear water condition. The tip-bed velocity was the main factor affecting the turbine coefficient K_t. Figure 16 shows the relationship between the tidal turbine scouring and tip-bed velocity. Two linear relationships were formed between the scour depth and tip-bed velocity. It can be seen that the scour depth was linear with the increase of velocity, and it no longer increased when the tip clearance was less than 0.50 D_t. The turbine coefficient K_t is related to tip-bed velocity and free flow velocity in the tip clearance range between 0.50 D_t and 1.00 D_t. K_t was obtained by the regression analysis from the experimental measurements, as shown in Equation (20)

$$K_t = 14.15 \frac{V_{tb}}{V_\infty} - 13.76 \quad C \geq 0.50 D_t \tag{20}$$

where V_{tb} is the tip-bed velocity (m/s) and V_∞ is the free flow velocity (m/s). The tidal turbine scour depth no longer increased when tip clearance was less than 0.50 D_t. K_t was considered a constant to produce Equation (21) when dimensionless the tip-bed velocity V_{tb}/V_∞ was larger than 1.14:

$$K_t = 1.6 \quad C < 0.50 D_t \tag{21}$$

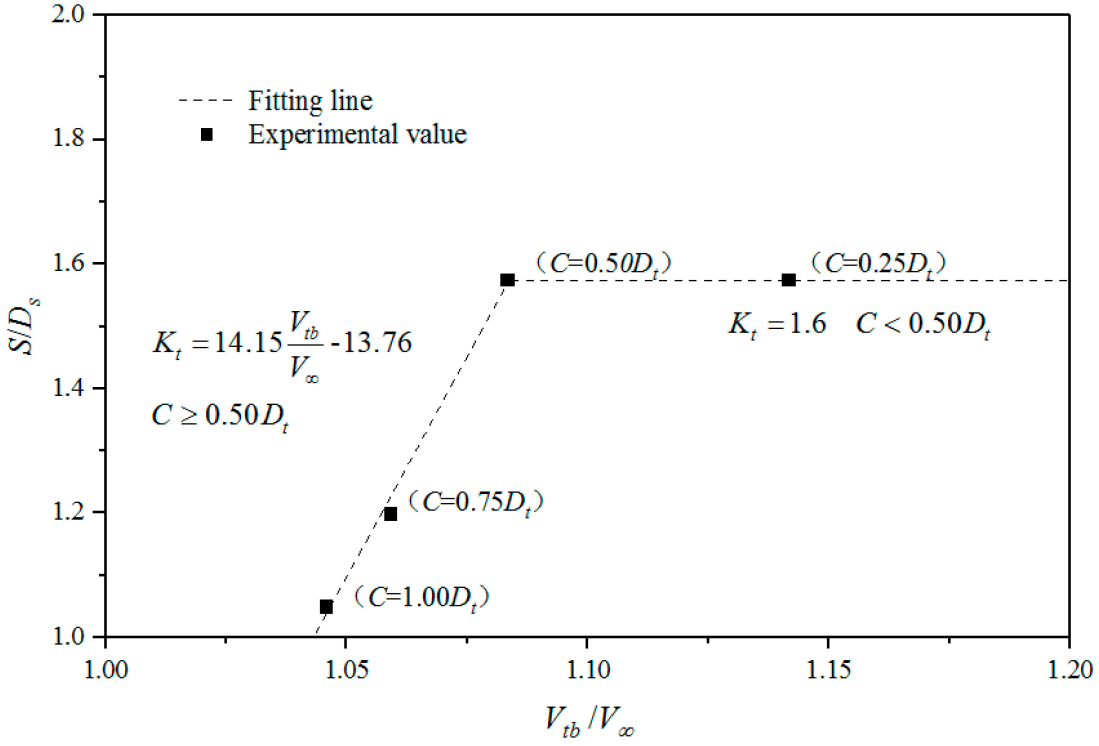

Figure 16. The relationship between the tip-bed velocity and tidal turbine scour depth.

The predicted tidal turbine scour depth was compared to the experimental measurement at various tip-bed clearances, as listed in Table 6. The predicted scour and the experimental measurements show good agreement, as shown in Figure 17. The maximum variation of 24.72% occurred in results from Chen [38]'s 0.50 D_t clearance case, which may be related to the influence of the tip speed ratio (TSR) of the tidal turbine. Generally, the empirical equation could estimate the seabed scour of a tidal turbine within a 30% error range. Based on Hill et al. [22], and Chen [38] results, the statistical functions using correlation coefficient (R), mean absolute error (MAE), root mean squared error (RSME), and scatter index (SI) in Equations (22)–(25) [40–42] were calculated to evaluate the performance and accuracy of Equation (19).

$$R^2 = \frac{\sum_{i=1}^{M}\left(O_i-\overline{O}\right)\left(P_i-\overline{P}\right)}{\sqrt{\sum_{i=1}^{M}\left(O_i-\overline{O}\right)^2\sum_{i=1}^{M}\left(P_i-\overline{P}\right)^2}} \tag{22}$$

$$MAE = \frac{1}{M}\sum_{i=1}^{M}\left|\frac{P_i-O_i}{O_i}\right| \tag{23}$$

$$RMSE = \left\{\frac{\sum_{i=1}^{M}|P_i-O_i|^2}{M}\right\}^{1/2} \tag{24}$$

$$SI = \frac{\sqrt{(1/M)\sum_{i=1}^{M}\left(\left(P_i-\overline{P}\right)-\left(O_i-\overline{O}\right)\right)^2}}{(1/M)\sum_{i=1}^{M}O_i} \tag{25}$$

where O_i is the experimental value, P_i is the predicted value from the equation, $\overline{O}$ is the average of the experimental value, $\overline{P}$ is the average of the predicted value, and M is the number of experimental points.

The predicted scour from the proposed equation fits well with the experimental data from the results of the statistical functions in Table 7. Berusers et al. [8], Richardson et al. [10], and Raaijmakers and Rudolph [39] improved Neil's cylindrical scour equation [7] with a consideration of water depth, flow angle, seabed conditions, and the size of bed material. The turbine coefficient K_t can also be

included in other cylinder scour equations (Berusers et al. [8], Richardson et al. [10], and Raaijmakers and Rudolph [39]) to estimate turbine scour.

Table 6. Seabed scour depth at various tip clearances.

Clearance	Source	Predicted Scour Depth (S/D_s)	Measured Scour Depth (S/D_s)	Variation
0.35 D_t	Hill et al. (2014) [22]	1.95	2.04	4.62%
0.50 D_t	Chen (2017) [38]	1.56	1.48	5.13%
0.75 D_t	Chen (2017) [38]	1.22	1.28	4.92%
1.00 D_t	Chen (2017) [38]	1.03	1.28	24.27%

Table 7. Error analysis.

Equation	R	MAE	RMSE	SI
$\frac{S}{D} = K_s K_t$	0.944	0.085	0.142	0.081

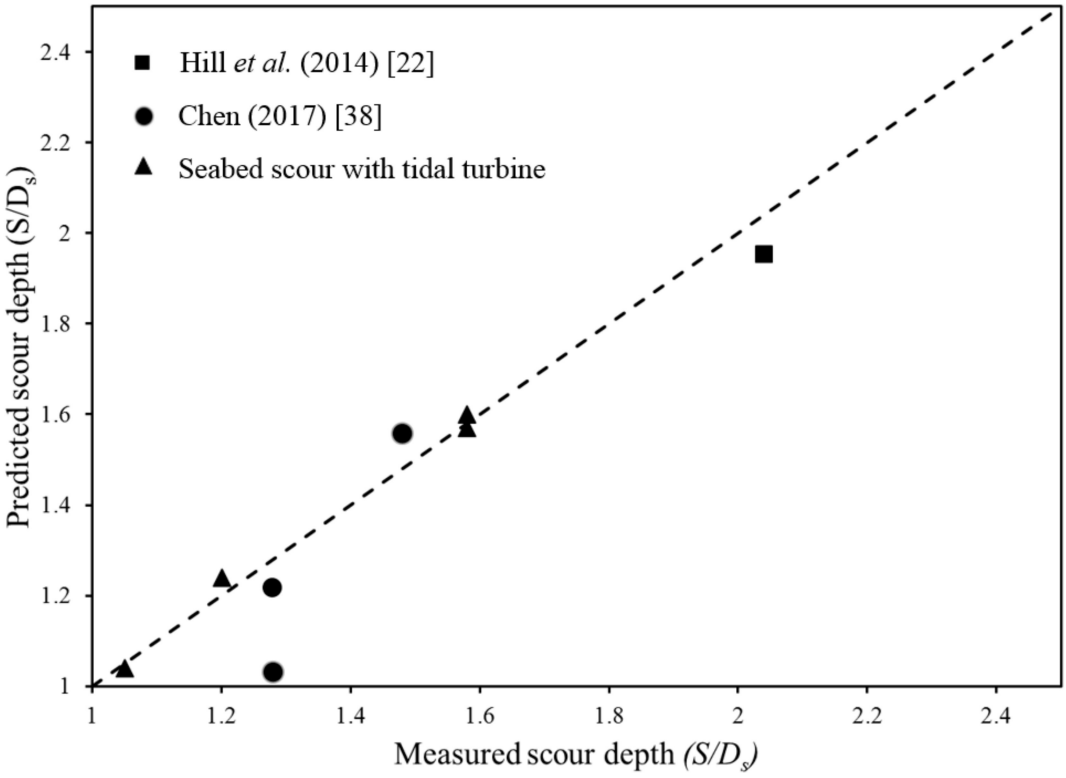

Figure 17. Scattered plot of measured and predicted seabed scour depth.

6. Conclusions

This research demonstrates the scour profile for horizontal-axis tidal turbines using theoretical and experimental investigations. An experimental apparatus was built to investigate tidal turbine scouring at various clearances in between the blades and seabed. The maximum scour depth, length of scour pit, and height of the deposited dune are presented through experimental measurements at different times. Tip-bed velocity, the accelerated velocity in between the blades and turbine, was studied in this research. The existence of a turbine leads to the flow acceleration of the tip-bed velocity and intensifies the seabed scour. Scouring experiments were conducted around a horizontal-axis tidal turbine with different tip clearances in a steady current. The conclusions are:

(1) A tip-bed velocity equation is proposed to estimate the seabed scour of a tidal turbine. The derivation of the equation is based on the axial momentum theory and conservation

of mass. In the calculation of a single case (Chen and Lam [5]), the proposed equation showed the variation was less than 4% for various tip clearances.

$$V_{tb} = V_\infty + \pi C_m r\left(\frac{V_\infty - V_0}{4C + (4-\pi)r}\right)$$

(2) A turbine significantly impacts its seabed scour due to shadowing effects. The influence of a turbine on scouring depends on the tip-bed clearance in between the blades and seabed. Scour depth is inversely proportional to tip clearance. The influence of a turbine is less significant when the clearance is excessively high ($C > 1.00\ D_t$) due to less significant shadowing effects. The influence of a turbine is the same even with smaller clearance after $C < 0.50\ D_t$ due to less blocked water diverting into the narrow region.

(3) An empirical equation is proposed to estimate the maximum tidal turbine scour depth. The turbine coefficient (K_t) is proposed to estimate the seabed scour depth of a tidal turbine with a consideration of the tip-bed velocity. The predicted data are well correlated with measured scour depth within a 5–24% error range. The correlation coefficient (R), mean absolute error (MAE), root mean squared error (RSME), and scatter index (SI) are 0.944, 0.085, 0.142, and 0.081, respectively.

$$\frac{S}{D} = K_s K_t$$

$$K_t = 14.15\frac{V_{tb}}{V_\infty} - 13.76 \quad C \geq 0.50 D_t$$

$$K_t = 1.6 \quad C < 0.50 D_t$$

(4) A mass flow coefficient (C_m) is proposed in the tip-bed velocity equation to include the blockage and shadowing effects to increase the flow velocity close to the seabed. In this paper, a mass flow coefficient (C_m) of 0.25 was used based on the assumption that 25% water flows downward into the mixing area. Water can flow upward, downward, leftward, and rightward. This 0.25 coefficient assumption allows for the predictions of tidal turbine scour depth by using the combined pile scour equation and tip-bed velocity equation. The mass flow coefficient (C_m) is influenced by various factors including flow velocity, flow turbulence, turbine position, and turbine parameters. The mass flow coefficient is complicated, and future research is needed.

Author Contributions: W.H.L.'s long term research series in ship propeller jet-induced scour and tidal turbine wake-induced scour; T.Z. and W.H.L. contributed to establish the tip-bed velocity equation and the scour mechanism for the horizontal-axis tidal turbine; T.Z. wrote the manuscript with revisions, recommendations and validations from W.H.L., Y.C., J.J., C.S., J.G., Y.M., S.W, S.S.L. and G.H.

Funding: This research was funded by the Natural Science Foundation of Tianjin City: 18JCYBJC21900 and Science Fund for Creative Research Groups of the National Natural Science Foundation of China (Grant no. 51621092). The APC was funded by the Natural Science Foundation of Tianjin City: 18JCYBJC21900.

Acknowledgments: The authors wish to extend their gratitude to the School of Civil Engineering at Tianjin University for laboratory space; Queen's University Belfast, University of Plymouth, University of Oxford, Dalian University of Technology, University of Malaya (HIR ENG47), Universiti Teknologi Malaysia, and Southern University College for their past support; and professional bodies EI, IEI, IET, BCS, IEM, IEAust, ASCE, ECUK, SCUK, BEM, FEANI, AFEO, MINDS and academy AAET for membership support and available resources.

Conflicts of Interest: The authors declare no conflict of interest.

Appendix A Correction Factor for Piles or Pier Equations

$K_s = \begin{matrix} 1.1 \\ 1.0 \\ 0.9 \end{matrix} \begin{matrix} \text{(Square nose)} \\ \text{(Round nose)} \\ \text{(Sharp nose)} \end{matrix}$	S is maximum scour depth (m).
$K_\theta = \left(cos\theta + \frac{L}{a}\sin in\theta\right)^{0.65}$	D is pile diameter (m).
$K_b = 0,\ if\ \frac{U_c}{U_{cr}} < 0.5$	h is pile height (m).
$K_b = 2\left(\frac{U_c}{U_{cr}}\right) - 1,\ if\ 0.5 \le \frac{U_c}{U_{cr}} < 1$	Ks is correction factor of pier shape.
$K_b = 1,\ if\ \frac{U_c}{U_{cr}} \ge 1$	K_θ is correction factor for flow angle.
$K_d = 1,\ if\ d_{50} < 2\text{mm}\ or\ d_{95} < 20\text{mm}$	K_b is correction factor for bed condition.
$K_d = 0.4U_*,\ if\ d_{50} \ge 2\text{mm}\ or\ d_{95} \ge 20\text{mm}$	K_d is correction factor for size of bed material.
$K_v = 1 - \exp(-A)$	K_v is correction factor accounting for wave action.
$K_h = \left(\frac{h_p}{h}\right)^{0.67}$	K_h is the correction factor accounting for piles that do not extend over the entire water column.

Nomenclature

V_0	efflux velocity in m/s
V_∞	free flow velocity in m/s
V_{tb}	tip-bed velocity in m/s
U_1–U_4	axial velocity in m/s at location 1–4
P_1–P_4	pressure in Pa at location 1–4
T	trust acted on actuator disc in N
C_T	thrust coefficient
C_m	flow mass coefficient
A	area of the actuator disc
A_1	area of water flowing through the actuator disc at location 1
ρ	density of fluid in kg/m^3
m	quality of the flow through the turbine in kg
m_1	total flow quality in the area A at location 1
Δm	fluid quality that has not passed through the actuator disc
Δm_1	downward flow mass
ΔP	energy change of water flow
C	tip clearance between turbine and seabed in m
r	radius of actuator disc in m
h_f	water depth of recirculating flume in m
D_t	diameter of turbine in m
D_s	Diameter of support structure in m
L_w	Width of water channel in m
L_d	Depth of water channel in m
d_{50}	Mean sediment grain diameter in mm
D	pile diameter in m
h	pile height in m
S	scour depth for turbine
K_s	correction factor of pier shape
K_t	correction factor of turbine

References

1. Watchorn, M.; Trapp, T. Chapter 585—Tidal Stream Renewable Offshore Power Generation (TS-Ropg). In Proceedings of the Energy for the 21st Century World Renewable Energy Congress VI 2000, Brighton, UK, 1–7 July 2000; Elsevier: Amsterdam, The Netherlands, 2000; pp. 2664–2667. [CrossRef]
2. Bonar, P.A.J.; Schnabl, A.M.; Lee, W.K.; Adcock, T.A. Assessment of the Malaysian tidal stream energy resource using an upper bound approach. *J. Ocean Eng. Mar. Energy* **2018**, *4*, 99–109. [CrossRef]

3. Rourke, F.O.; Boyle, F.; Reynolds, A. Marine current energy devices: Current status and possible future applications in Ireland. *Renew. Sustain. Energy Rev.* **2010**, *14*, 1026–1036. [CrossRef]
4. Chen, L.; Lam, W.H. Methods for predicting seabed scour around marine current turbine. *Renew. Sustain. Energy Rev.* **2014**, *29*, 683–692. [CrossRef]
5. Chen, L.; Lam, W.H. Slipstream between marine current turbine and seabed. *Energy* **2014**, *68*, 801–810. [CrossRef]
6. Sumer, B.M.; Christiansen, N.; Fredsoe, J. *Time Scale of Scour around a Vertical Pile*; International Society of Offshore and Polar Engineers: Mountain View, CA, USA, 1992; ISBN 1-880653-03-6.
7. Neill, C.R. *Roads and Transportation Association of Canada. Project Committee on Bridge Hydraulics. Guide to Bridge Hydraulics*; University of Toronto Press: North York, ON, Canada, 1973; ISBN 0802019617.
8. Breusers, H.N.C.; Nicollet, G.; Shen, H.W. Local scour around cylindrical piers. *J. Hydraul. Res.* **1977**, *15*, 211–252. [CrossRef]
9. Sumer, B.M.; Fredsøe, J.; Christiansen, N. Scour Around Vertical Pile in Waves. *J. Waterw. Port Coast. Ocean Eng.* **1992**, *118*, 15–31. [CrossRef]
10. Richardson, E.V.; Harrison, L.J.; Richardson, J.R. *Evaluating Scour at Bridges*; Federal Highway Administration: Washington, DC, USA, 1993.
11. Albertson, M.L.; Dai, Y.B.; Jensen, R.A.; Rouse, H. Diffusion of Submerged Jets. *Am. Soc. Civ. Eng.* **1950**, *115*, 639–664. [CrossRef]
12. Hamill, G.A. Characteristics of the Screw Wash of a Manoeuvring Ship and the Resultant Bed Scour. Ph.D. Thesis, Queens University of Belfast, Belfast, UK, 1987.
13. Lam, W.H.; Hamill, G.A.; Robinson, D.J.; Raghunathan, S. Semi-empirical methods for determining the efflux velocity from a ship's propeller. *Appl. Ocean Res.* **2012**, *35*, 14–24. [CrossRef]
14. Jiang, J.X.; Lam, W.H.; Cui, Y.G.; Zhang, T.M.; Sun, C.; Guo, J.H.; Ma, Y.B.; Wang, S.G.; Hamill, G. Ship Twin-propeller Jet Model used to Predict the Initial Velocity and Velocity Distribution within Diffusing Jet. *KSCE J. Civ. Eng.* **2019**, *23*, 1118–1131. [CrossRef]
15. Hamill, G.A. *Scouring Action of the Propeller Jet Produced by a Slowly Manoeuvring Ship*; Bulletin of the Permanent International Association of Navigation Congresses [PIANC]: Brussels, Belgium, 1988.
16. Hamill, G.A.; Johnston, H.T.; Stewart, D.P. Propeller Wash Scour near Quay Walls. *J. Waterw. Port Coast. Ocean Eng.* **1999**, *125*, 170–175. [CrossRef]
17. Cui, Y.G.; Lam, W.H.; Zhang, T.M.; Sun, C.; Hamill, G. Scour Induced by Single and Twin Propeller Jets. *Water* **2019**, *11*, 1097. [CrossRef]
18. Lam, W.H.; Chen, L.; Hashim, R. Analytical wake model of tidal current turbine. *Energy* **2015**, *79*, 512–521. [CrossRef]
19. Ma, Y.B.; Lam, W.H.; Cui, Y.G.; Zhang, T.M.; Jiang, J.X.; Sun, C.; Guo, J.H.; Wang, S.G.; Lam, S.S.; Hamill, G. Theoretical vertical-axis tidal-current-turbine wake model using axial momentum theory with CFD corrections. *Appl. Ocean Res.* **2018**, *79*, 113–122. [CrossRef]
20. Schluntz, J.; Willden, R.H.J. The effect of blockage on tidal turbine rotor design and performance. *Renew. Energy* **2015**, *81*, 432–441. [CrossRef]
21. Sun, C.; Lam, W.H.; Lam, S.S.; Dai, M.; Hamill, G. Temporal Evolution of Seabed Scour Induced by Darrieus-Type Tidal Current Turbine. *Water* **2019**, *11*, 896. [CrossRef]
22. Hill, C.; Musa, M.; Chamorro, L.P.; Ellis, C.; Guala, M. Local Scour around a Model Hydrokinetic Turbine in an Erodible Channel. *J. Hydraul. Eng.* **2014**, *140*, 04014037. [CrossRef]
23. Sun, C.; Lam, W.H.; Cui, Y.; Zhang, T.; Jiang, J.X.; Guo, J.H.; Ma, Y.B.; Wang, S.G.; Tan, T.H.; Chuah, J.H.; et al. Empirical model for Darrieus-type tidal current turbine induced seabed scour. *Energy Convers. Manag.* **2018**, *171*, 478–490. [CrossRef]
24. Giles, J.; Myers, L.; Bahaj, A.; O'Nians, J.; Shelmerdine, B. Foundation-based flow acceleration structures for marine current energy converters. *IET Renew. Power Gener.* **2011**, *5*, 287–298. [CrossRef]
25. Wang, S.G.; Lam, W.H.; Cui, Y.G.; Zhang, T.M.; Jiang, J.X.; Sun, C.; Guo, J.H.; Ma, Y.B.; Hamill, G. Novel energy coefficient used to predict efflux velocity of tidal current turbine. *Energy* **2018**, *158*, 730–745. [CrossRef]
26. Hamill, G.A.; Mcgarvey, J.A.; Hughes DA, B. Determination of the efflux velocity from a ship's propeller. *Proc. ICE Marit. Eng.* **2004**, *157*, 83–91. [CrossRef]
27. Lam, W.H.; Chen, L. Equations used to predict the velocity distribution within a wake from a horizontal-axis tidal-current turbine. *Ocean Eng.* **2014**, *79*, 35–42. [CrossRef]

28. Lam, W.H.; Guo, J.H.; Jia, S.R.; Tian, Y.F. A Horizontal Recirculating Flume for Tidal-Current-Turbine. China Patent CN106124161A, 16 November 2016.
29. Bahaj, A.S.; Molland, A.F.; Chaplin, J.R.; Batten, W.M.J. Power and thrust measurements of marine current turbines under various hydrodynamic flow conditions in a cavitation tunnel and a towing tank. *Renew. Energy* **2007**, *32*, 407–426. [CrossRef]
30. Myers, L.E.; Bahaj, A.S. Experimental analysis of the flow field around horizontal axis tidal turbines by use of scale mesh disk rotor simulators. *Ocean Eng.* **2010**, *37*, 218–227. [CrossRef]
31. Gaurier, B.; Germain, G.; Facq, J.V.; Johnstone, C.M.; Grant, A.D.; Day, A.H.; Nixon, E.; Di Felice, F.; Costanzo, M. Tidal energy Round Robin" tests comparisons between towing tank and circulating tank results. *Int. J. Mar. Energy* **2015**, *12*, 87–109. [CrossRef]
32. Rambabu, M.; Rao, S.N.; Sundar, V. Current-induced scour around a vertical pile in cohesive soil. *Ocean Eng.* **2003**, *30*, 893–920. [CrossRef]
33. Whelan, J.I.; Graham, J.M.R.; Peiró, J. A free-surface and blockage correction for tidal turbines. *J. Fluid Mech.* **2009**, *624*, 281–291. [CrossRef]
34. Yu, C.L. The System Design and parameter Study of Circulating Water Channel. Master Thesis, Harbin Engineering University, Harbin, China, 2009. (In Chinese).
35. Zhao, M.; Cheng, L.; Zang, Z. Experimental and numerical investigation of local scour around a submerged vertical circular cylinder in steady currents. *Coast. Eng.* **2010**, *57*, 709–721. [CrossRef]
36. Kitsikoudis, V.; Kirca, V.O.; Yagci, O.; Celik, M.F. Clear-water scour and flow field alteration around an inclined pile. *Coast. Eng.* **2017**, *129*, 59–73. [CrossRef]
37. Yao, W.; An, H.; Draper, S.; Cheng, L.; Harris, J.M. Experimental investigation of local scour around submerged piles in steady current. *Coast. Eng.* **2018**, *142*, 27–41. [CrossRef]
38. Chen, L. Wake of Horizontal Axis Tidal Current Turbine and Its Effects on Scour. Ph.D. Thesis, University of Malaya, Kuala Lumpur, Malaysia, 2017.
39. Raaijmakers, T.; Rudolph, D. Time-dependent scour development under combined current and waves conditions-laboratory experiments with online monitoring technique. In Proceedings of the 4th International Conference on Scour and Erosion (ICSE-4), Tokyo, Japan, 5–7 November 2008; pp. 152–161.
40. Najafzadeh, M.; Balf, M.R.; Tafarojnoruz, A. Prediction of riprap stone size under overtopping flow using data-driven models. *Int. J. River Basin Manag.* **2018**, *16*, 505–512. [CrossRef]
41. Najafzadeh, M.; Shiri, J.; Rezaiebalf, M. New expression-based models to estimate scour depth at clear water conditions in rectangular channels. *Mar. Georesour. Geotechnol.* **2017**, *36*, 227–235. [CrossRef]
42. Najafzadeh, M.; Barani, G.; Hessami, M.R.H. Estimation of pipeline scour due to waves by GMDH. *J. Pipeline Syst. Eng. Pract.* **2014**, *5*. [CrossRef]